ELSEVIER

Contents lists available at ScienceDirect

Composites Part B

journal homepage: www.elsevier.com/locate/compositesb



Check for updates

Metal organic frameworks modification of carbon fiber composite interface

S. Ayyagari a, M. Al-Haik a, Y. Ren b, A. Abbott b, E.B. Trigg b, B. Zheng b, H. Koerner b

- Department of Aerospace Engineering, Embry-Riddle Aeronautical University, Daytona Beach, FL, USA
- b Materials and Manufacturing Directorate, Air Force Research Laboratory (AFRL/RXCC), Wright-Patterson AFB, OH, USA

ARTICLE INFO

Keywords: Carbon fibera Metal organic frameworka Carbon nanotubea Adhesion Composite

ABSTRACT

Carbon fiber reinforced polymeric composites (CFRPs) are prone to delamination due to insufficient interfacial properties. Several remedies were carried out to enhance the fiber/matrix interfaces via chemical treatments or utilizing stiffer nanomaterials at the interface. However, some of these treatments are destructive in nature and others are non-scalable. This investigation corroborates a novel methodology for developing hybrid reinforcements that comprise carbon fibers and metal organic frameworks (MOFs). The growth of MOFs is scalable, non-destructive to the fibers, and easily tailorable to control the porous morphologies of the MOFs at the interface. Furthermore, the study demonstrates the feasibility of utilizing the MOFs as a catalyst to grow carbon nanotubes (CNTs) on the carbon fibers. The microstructure of the MOFs was examined via microscopy, Raman analysis, wide-angle X-Ray scattering (WAXS), and Fourier-transform infrared spectroscopy (FTIR). The effects of the MOFs on the fiber thermal stability was probed using thermogravimetric analysis (TGA), while contact angle analysis was employed to probe the effect of the different surface modifications on the fibers hydrophilicity. Several mechanical characterizations including tensile, dynamic mechanical analysis (DMA) and shear lap joint were carried out to discern the effects of the MOFs on the composite structural performance. Several improvements emanated from the MOFs placement on the interface including improving the strength, enhancing the damping parameter by 500%, increasing the glass transition temperature of the composite by 20 °C and alleviating the shear lap joint strength by 40%.

1. Introduction

Carbon fiber reinforced polymeric composites (CFRPs) have found numerous applications in a plethora of industries spanning from aerospace to sporting goods due to their superior structural performance, light weight, and ease of manufacturing. The addition of the carbon fibers to thermosets or thermoplastic matrices enables a spectrum of properties that capitalize on the fibers' elevated strength and stiffness, and the matrix toughness and ductility. However, this filling process also introduces new interfaces between the two constituents, which carry a profound impact on the composite performance and properties [1]. The interface can be thought of as a shared geometric surface between the fiber and the matrix, whose main purpose is to establish sufficient bonding between the two constituents such that the load can transfer efficiently from the matrix to the fiber. The interface is often considered as a separate phase by itself with properties different from those of the fiber and the matrix. Hence, sometimes it is called "interphase" [2]. Thorough reviews to study the chemical composition and the properties of the interfaces in CFRPs are available [2-6]. It was determined that the smooth surfaces and low chemical activation of untreated carbon fibers result in inadequate interfacial strength in the composite, which propelled the need for surface treatment of the carbon fibers. Some of the remedies applied to the carbon fibers to enhance the interface adhesion include acid treatments [7,8], controlled anodic oxidation [9,10], and placement of nanophases on the fiber surface [11-14]. Fu et al. [10], reported significant improvements on the interlaminar shear strength of carbon fiber composites upon treating them via acid oxidation, followed by electrochemical grafting of diethylenetriamine (DETA). Yao et al. [14] utilized chemical vapor deposition (CVD) to grow carbon nanotubes (CNTs) on carbon fibers, and reported a 30.73% and 32.29% improvement in the interfacial shear strength and interlaminar shear strength, respectively, of their derived composites. However, other studies suggested that growing CNTs via CVD, the elevated temperatures in the reactor degraded the tensile strength significantly [15]. Identically, some investigations reported that the tensile properties of composites based on carbon fibers with hydrothermally grown ZnO

E-mail address: alhaikm@erau.edu (M. Al-Haik).

^{*} Corresponding author.

nanowires could affect the strength and stiffness negatively due to unrecovered moisture absorption [13].

In lieu of CNTs and ceramic nanowires growth on the carbon fibers, recent investigations advocated the metallization of carbon fibers. There are several techniques for metal deposition on different substrates, including CVD, magnetron sputtering, and via deposition of metal organic framework (MOFs). CVD is the most utilized technique for metalizing carbon fibers to be used as reinforcements in metal matrix composites. Abidin et al. [16], utilized CVD with a mixture of TiCl₄, N₂ and H2 gases to deposit titanium nitride on carbon fiber textile, prior to embedding this hybrid reinforcement in aluminium matrix. The magnetron sputtering, also referred to as physical vapor deposition (PVD), entails deposition of nanometres-thick metallic films via creating a gaseous plasma, and accelerating its ions into a metal target, upon which the target will erode and eject clusters of atoms that are deposited on the carbon fibers. This technique was mostly utilized for the deposition of the catalytic metals needed to grow CNTs on the surface of carbon fibers, such as nickel [17 19]. Both CVD and PVD lack the scalability required for CFRPs, due to the limited sample size and the need for high vacuum or elevated temperatures.

A metal organics framework (MOF) is a three-dimensional structure that comprises metal ions coordinated to organic ligands. These structures are very porous with large surface area [20]. The utilization of MOFs with carbon materials was mostly for non-structural applications such as catalysis, gas adsorption or enhanced transport properties. For example, Tran et al. [21], formed a porous catalyst that comprised of CNTs and metal organic frameworks (MOFs) for the detection of urea, while Yan et al. [22], utilized graphene coated with MOFs as an effective water splitting electro-catalyst. Bhoria et al. [23], utilized copper-based MOF hybridized with graphene oxide for adsorption of toxic $\rm H_2S$ gas and observed 27% improvement in the adsorption capacity, over that for neat graphene oxide.

The use of MOFs with both porous and nano carbon materials is very diverse. Kim eta l., [24], synthesized porous carbon via simple pyrolysis of zinc- MOFs toward $\rm CO_2$ capture and found that its capacity is far better than that based on pristine MOFs. Identically, MOFs/nanocarbons were also utilized for hydrogen storage [25]. Liu et al., carbonized Al-based MOFs toward preparing carbon nanosheets for super capacitors [26]. Identical use of MOFs and nano-porous carbon in supercapacitors were reported by several research groups [27,28]. Porous carbon nanofibers were fabricated using MOFs as hybrids by electrospinning and calcination [29]. These hybrids were implemented in lithium-ion batteries yielding superior capacity and charging rate due to the fast ion/electron path and huge contact surfaces furnished by the porous nanofibers. Lithium-suffer batteries also benefited from combinations of MOFs and nano-porous carbons [30].

In lieu of ceramic or carbonaceous interfacial nano species, in this investigation we utilized MOFs to modify the surface of structural carbon fibers toward amplifying the interfacial properties of CFRPs. Also, we probed utilizing the nickel-based MOFs as catalyst to grow CNTs on the carbon fibers. Different mechanical and microstructural techniques were implemented to reveal the performance and the microstructure of these surface treatments on the derivative composites.

2. Materials and experimental methods

The carbon fibers utilized were unsized, plain woven, structural, polyacrylonitrile (PAN) grade, Thornel-650 (Cytec, Inc.), with 3k bundles. To allow the formation of active cites (-COOH), the fibers were cut into 6 $\,$ 6 squares and were treated in a diluted mix (2:1) of de-ionized (DI) water/HNO $_3$ acid for 24 h. The fibers were rinsed thoroughly with DI water till a pH of 7.0 was achieved, followed by drying in an oven at 100 $\,$ C for 24 h.

To prepare the MOFs growth mixture, one solution was made by dissolving the metal ion source; nickel nitrate hexahydrates (Ni $(NO_3)_2$ $6H_2O$, Sigma Aldrich Co.) in 100 mL of methanol to yield a 0.65

M concentration. The ligands solution was made by dissolving 2-methylimidazole ($C_4H_6N_2$, Sigma Aldrich Co) in 100 mL of methanol: 0.14 M concentration. Each solution was magnetically stirred, separately, at 400 rpm for 6 h, then the two solutions were magnetically stirred together for 10 min. A single carbon fiber cloth was immersed in the solution for 24 h, while suspended, to allow MOFs deposition on both surfaces. The carbon fiber cloth was removed from the solution and washed repeatedly with methanol then left to dry in an oven at 100 $\,$ C for 24 h

While the focus of this study is on the MOFs effects on the interface, we extended the experiments to examine the feasibility of the nickel-based MOF as a catalyst to grow CNTs; as an alternative to PVD deposition of the catalyst in other investigations [17–19]. The CNTs growth was performed inside a quartz tube reactor, outfitted with a thermal controller and three-input gas (N₂, C₂H₂ and H₂) mass flow controllers (MKS Co.). The process begins with a reduction step to remove excessive oxides from the MOFs by flowing H₂/N₂ gas mixture atmosphere at 550 C for 2 h. Then, the tube reactor is flushed with N₂ gas to get rid of any residuals of the previous step. Subsequently, the CNTs growth step begins, maintaining the constant temperature of 550 C, for 30 min under a balanced $C_2H_4/H_2/N_2$ environment.

Raman spectroscopy analysis of the modified fibers was carried out utilizing PeakSeekerPro (Raman Systems, Inc), with excitation wavelength of 532 nm and laser power of 100 W. The microstructures and morphologies of the carbon fibers with different surface treatments were characterized utilizing scanning electron microscopy (SEM, FEI Quanta 650, Thermo Fisher Scientific Co.) equipped with energy-dispersive X-ray spectroscopy (EDS) detector (Bruker, Inc.) A Zeiss Gemini 500 scanning transmission electron microscope (STEM) was utilized to further investigate the MOFs pre and post reduction to examine the size and elemental composition of the particles utilized as catalyst to grow the CNTs.

To examine the effect of the different processes on the surface of the carbon fibres, wide-angle X-ray diffraction (WAXD) was performed using a Xeuss 3.0 (Xenocs Inc.) The X-ray wavelength was 1.54 Å, the sample-to-detector distance was 55 mm, and the exposure time was 1 h. Samples were taped directly to a sample holder such that no substrate or capillary was needed. A Pilatus3 300k detector was used to collect scattered X-rays. Two-dimensional scattering patterns were analysed using the Datasqueeze software [31]. To obtain the 1D scattering curves, all 2D scattering patterns were integrated over a 90 wedge parallel to the fiber axis. Scattering perpendicular to the fiber axis was excluded from the integration.

The presence of functional groups on the different fibers configurations was studied using Fourier transform infrared spectroscopy (FTIR, Nicolet 380) at wavelengths of 600 4000 cm $^{-1}$ using the attenuated total reflection (ATR) module.

The thermal stability of the different fibers configurations were examined using TA Q500 thermogravimetric analyzer (TGA). Single tow weighing around 7.5 mg of each fiber type was cut and placed inside the TGA platinum pan. The analyzer was programmed to ramp from RT to 850 C at 20 C/min under nitrogen environment.

To examine the effects of the different surface treatments on the wettability of the carbon fibers, contact angle measurements were carried out using the Attention Theta optical tensiometer (Biolin Scientific Co.) As the instrument optical zoom is limited and does not support measurement of the angle of contact for a single fiber, we implemented the procedures carried by Wang et al. [32] to measure the wettability of carbon fibers bundles at mesoscale. For each fiber s configuration, a tow was slowly soaked in DI water for 100 s to ensure the external meniscus around the tow reached a static configuration. A digital camera captured images of the external contact angle and the variation of the tow diameter.

Four different composites were fabricated based on the (i) reference fibers, (ii) acid-treated fibers, (iii) MOFs modified fibers, and (iv) fibers with surface grown CNTs. Each composite comprised two plies adhered

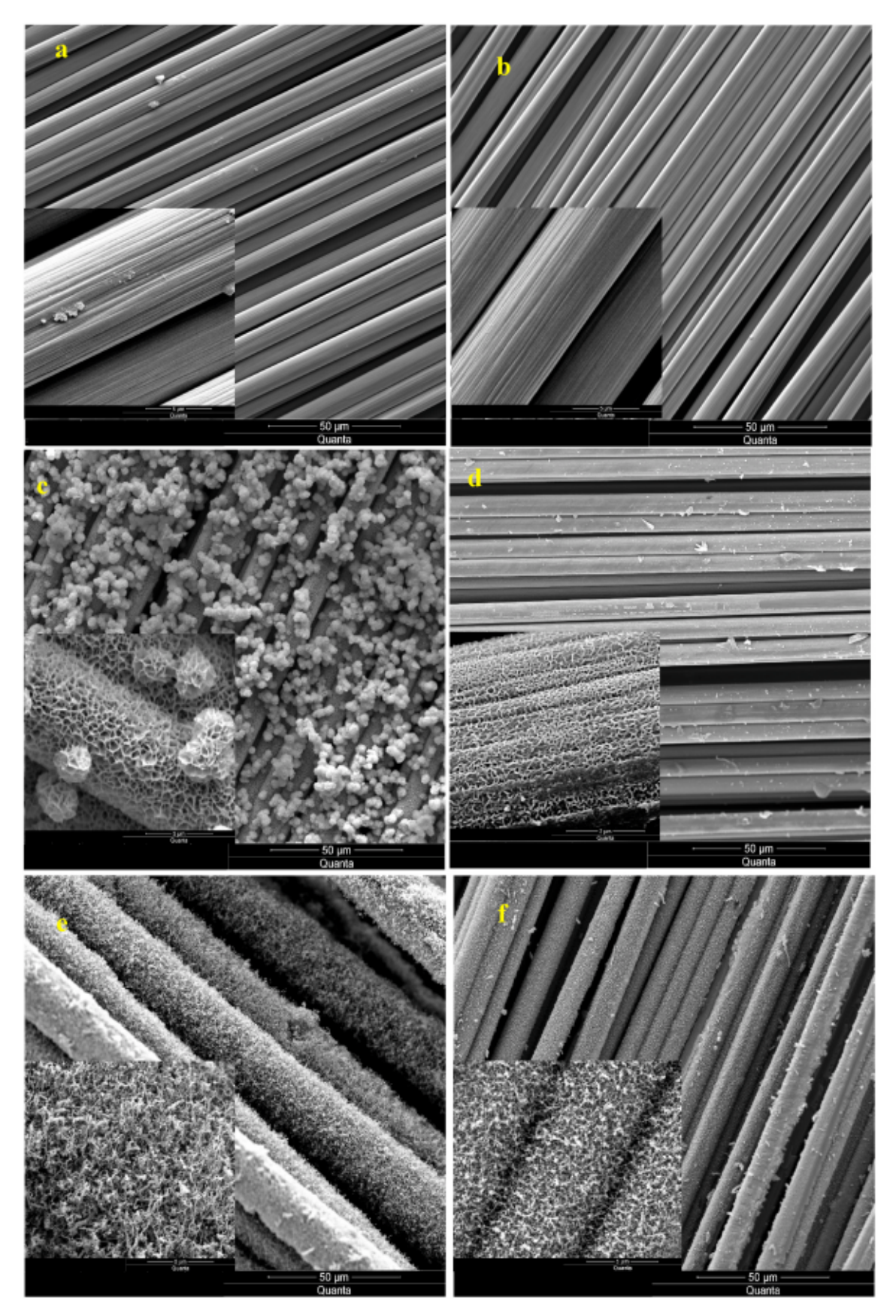


Fig. 1. Scanning electron microscopy (SEM) micrographs of T650 carbon fibers with different surface treatments (a) reference de-sized fibers, (b) acid treated, (c) MOFs growth with concentration of 0.65 M, (d) MOFs growth with concentration of 0.33 M, (e) CNTs growth based on the fibers with 0.65 M MOFs concentration, and (f) CNTs growth based on the fibers with 0.33 MOFs concentration.

8. Ayyagari et al. Composites Part B 224 (2021) 109197

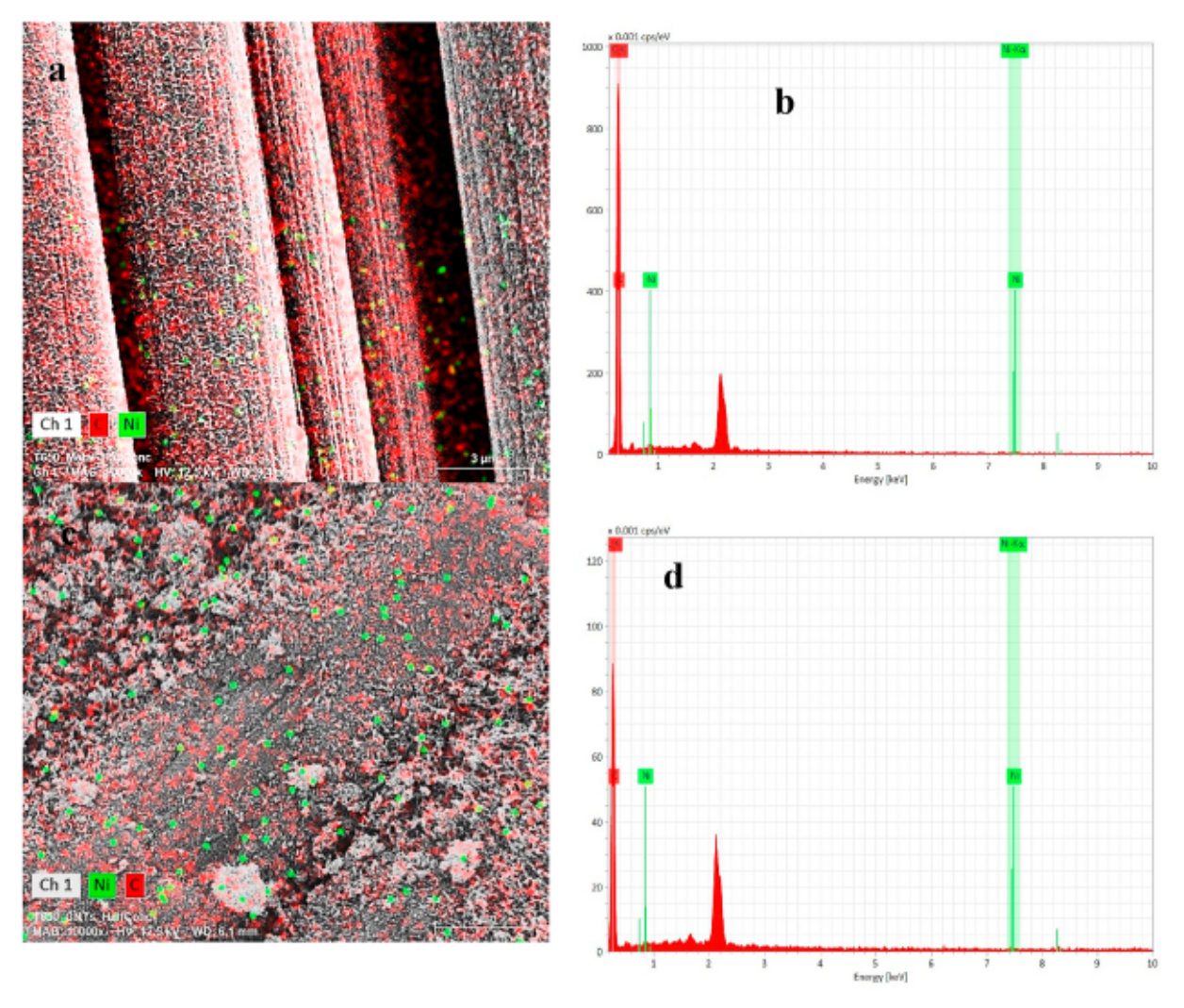


Fig. 2. EDS analysis of the carbon and nickel elemental analysis for (a-b) the carbon fibers with MOFs and (c-d) carbon fibers with MOF after growing CNTs.

by an epoxy matrix; Epon 862™; (Diglycidyl Ether of Bisphenol-F (Miller Stephenson, Co.) This resin is utilized for structural applications with a high viscosity of 2500-4500 cPs at 25 °C. The curing agent system is Epikure -WTM; an aromatic amine (Miller Stephenson, Co.) with room temperature viscosity of 100-300 cPs. When both the resin and hardener are mixed in a ratio of 100:26.4 by weight, a viscosity of 2100-2300 cPs and a gelling temperature of 177 °C were reported by the manufacturer. The hand-layup method was employed for lamination. For each fiber configuration two-plies laminae were impregnated with epoxy, with fiber to epoxy wight ratio of 60:40, were sealed in a vacuum bag. The vacuum bag containing the four composites laminates was placed inside an aerospace grade autoclave (Econoclave, ASC Co.) A vacuum of 25 torr was maintained inside the vacuum bag throughout the curing process. By flowing N2 in the autoclave chamber via twostage regulators, a pressure of 70 psi was obtained. The autoclave cycle had four segments: Isothermal step for 1.0 h at 25 °C, heating to 177 °C, isothermal step for 2.5 h at 177 °C, and finally cooling down to room temperature.

Different composites coupons were prepared for tensile, damping and shear lap tests. For tensile testing, coupons of 12.50 × 1.25 cm were prepared and tested following the ASTM standard D3039 utilizing an MTS Criterion™ Model 43 system (MTS, Inc.) equipped with a 25.4-mm gauge length extensometer to measure the strain. The tests were conducted under constant crosshead speed of 1.0 mm/min until failure occurred. Ten samples were tested for each composite configuration.

Dynamic mechanical analysis (DMA) testing was carried out utilizing

DMA8000 analyzer (PerkinElmer, Inc.), following the ASTM D5023-15 and ASTM D7028-07 standards. Composite beams of 50.00 mm \times 6.25 mm were used and a three-point bending fixture with a span of 40 mm was utilized to mount each of the composite samples. Through the DMA temperature sweep mode, a 1.0 Hz frequency was maintained, while sweeping the temperature from 30 to 170 °C while the beam is under a constant strain of 0.01 mm. The frequency sweep test was performed from 1 to 100 Hz under isothermal condition of at 25 °C using the same strain applied in the temperature sweep test, and a constant force of 1.0 N.

To assess the effect of the different fiber's surface treatments on their adhesion to the epoxy, four different sets of composites samples were prepared following the ASTM -D5868 standard for shear lap adhesion test specific to FRPs. Each specimen comprised eight plies to acquire the thickness recommended in the ASTM standard. While the outer six plies were made of reference carbon fibers with no surface treatments, the two intermediate plies at the joint were based on fibers with different surface treatments; reference, acid treated, MOFs, and CNTs. The samples were manufactured in the autoclave following the thermal cycle utilized for making the tensile and DMA samples. Upon curing and cutting the composites, each sample comprised two joints, each with the dimensions of 101.6 mm \times 25.4 mm \times 0.75 mm. The tow plies at each joint overlapped over an area of 25.4 mm × 25.4 mm. The shear lap samples, individually, were held inside the grips of the MTS testing system, allowing grip separation of 76.2 mm. Each sample was loaded in tension at a constant rate of 13 mm/min until the joint fails. Five

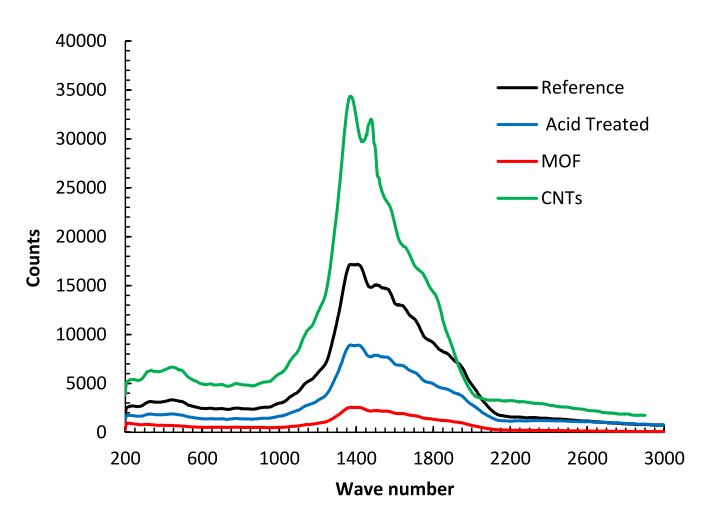


Fig. 3. Raman spectra of the T650 carbon fibers with different surface treatments.

samples were tested for each composite configuration.

3. Results and discussion

The micrographs of the carbon fibers with different surface treatments are shown in Fig. 1. Fig. 1(a) shows a flake resembling the removed sizing. Treating the fibers with the diluted HNO3 solution dissolved these peels; nitric acid is well known for introducing the carboxylic group (-COOH) to the fibers surface [33]. The acid treatment also plays an etching effect revealing several fibrils at the surface of the carbon fiber that can be seen in Fig. 1(b). Very organized MOFs porous structures emerged upon utilizing highly concentrated solution of the metal source as can be seen in Fig. 1 (c). The pores are separated by very thin sheet walls of the MOFs. A dense concentration of microscale spherical MOFs cages were observed to precipitate on the carbon fibers. These cages were a result of insufficient stirring of the metal salt initially, where large crystals of the metal salts, when left un-dissolved, become a substrate on their own leading to an array growth of MOFs cages which was reported by other studies as well [34]. It is worth mentioning that, while published literature displayed the presence of these thin MOFs sheets, they lacked the ordered pattern presented herein. Some of the patterns reported are solid cubical cages [35]. nanobelts [36] and microspheres [34]. Several factors play roles in the formation of the different patterns of the MOFs such as the metal source concentration, the ligand utilized, the growth duration and the substrate material. For example, upon reducing the metal seeding solution concentration by 50%, to 0.33 M, and upon following the same protocol it was clear from Fig. 1(d) that the well-defined thin sheet walls have

Utilizing MOFs as catalyst to grow CNTs is one of the objectives of the current investigation. As shown in Fig. 1(e), The dense MOFs deposition leads to very dense CNTs growth that enlarged the fiber diameters from 6.8 m, as reported by the manufacturer, to almost 30.0 m. Such dense growth hinders the resin ability to wet the fibers and penetrate through the bundles. The fibers with MOFs grown via 0.33 M seeding solution concentration yielded more uniform and less dense growth of CNTs as shown in Fig. 1(f). Such growth, from previous experience, allows for better flowability of the epoxy in between the fibers.

As shown in Fig. 2(a b), the energy-dispersive X-ray spectroscopy (EDS) of the carbon fibers with MOFs revealed strong peaks of crystal-line nickel. The EDS was carried out after the CNTs growth, Fig. 2(c d), the carbon peak became stronger because of the added CNTs atoms. Identically, the Ni spots became more contrasted since the reduction process, prior to the CNTs growth, assisted in removing oxides that might have been developed during the MOFs deposition.

The Raman spectra for the reference carbon fiber, shown in Fig. 3, revealed a strong disordered graphitic (D; 1360 cm⁻¹) peak and much weaker ordered graphitic (G; 1580 cm⁻¹) peak. A lesser referred to peak is the A peak roughly at 1500 cm⁻¹, which is indicative of amorphous carbon. The T650, being a PAN based fiber, is not highly graphitic and do not exhibit a G band. However, they display a D peak that corresponds to the structural disorder caused by the presence of the sp³ bonds [37]. Upon acid treatment, the intensities of both the D and G peaks reduced, also the G band was broadened and shifted to a higher frequency. This shift is attributed to the presence of the COOH functional groups on the surface [38]. Also, the reduction in the G band intensity is indicative of reduced number of graphitic layers. The change in the ratio of the peak s intensities (I_D/I_G) is indicative of the number of defects sites; the functional groups can be thought of as defects. The deposition of MOFs on the surface of the fiber basically masked the D and G peaks due to the higher coverage of metal crystals and the spectra is just a measure of the absorption of the MOFs. The suitability of the Raman analysis to carbon fibers coated with MOFs is yet to be determined. One of the few references on the use of Raman spectroscopy with Ni based MOF was limited only to analyses of the normal modes of the MOF lattice vibrations at terahertz (THz) region, that corresponds to low wave number region in Raman spectra [39]. Upon growing the CNTs on the surfaces of the T650 carbon fiber, a strong D-band at 1350 cm⁻¹ and G-band at 1595 cm 1 , are apparent. The intensity ratio (I_D/I_G) is more noticeable for the carbon fibers with CNTs, indicating a high degree of crystallinity due to their presence.

The WAXD patterns of the carbon fibers are show in Fig. 4(a). The patterns indicates a diffuse anisotropic scattering and the reference and acid treated fibers show a fan-like scattering which is typical for PAN based carbon fibers such as T650 [40] and AS4 [41]. Such scattering pattern arises from the random distribution of needle-like pores on the fibers; the intensity distribution in the reciprocal space comprises of disks cantered at the origin of that space with disks normal parallel to the principal axis of the pores [40]. Disk thickness is inversely related to the length of the pores. The fan-like shape is comprised of superposition of disks with finite thicknesses.

The reference and the acid treated fibers exhibit identical patterns indicating that the acid treatment did not alter the crystallinity of the fibers. This is anticipated as PAN fibers are typically prepared via charring of a resin that does not undergo a liquid crystal state. Hence, upon graphitizing, PAN fibers display a turbostratic carbon peak as can be observed in Fig. 4(b). The peak beyond 2 25 is typical of a turbostratic fibers and it appears in all samples as the fiber serve as a substrate for the different coatings. Upon carrying the MOFs synthesis, a different scattering pattern with many crystalline peaks emerges. This new crystalline phase apparently possesses a large unit cell as its scattering peaks do not match those of the Ni (111) crystallographic plane or NiO (200) and (111) planes. The MOF sample when reduced at 550 C under inert environment loses several of these peaks and shows a noticeable peak at 2 39 which is indicative of the NiO (111) plane. The sample with CNTs displays a maximum peak at 26.2 that corresponds to the wall-to wall periodicity in multi wall CNTs; it is a characteristic of the (002) reflection from the graphitic layer. WAXS confirmed that these are multi wall CNTs (MWCNTs) as single wall CNTs comprise single graphitic layer, while diffraction requires presence of several planes. The interspacing between the graphitic shells can be computed from d $\, \, 2 \, / q_{max} \, \, \, \, \, 3.40 \; A \,$ (where the scattering vector is given by a $4 \sin (2/2)$; is the wavelength) which agrees with those for standard graphite.

The FTIR spectra of the different fibers are shown in Fig. 5. The FTIR spectra of the reference carbon fibers do not show discernible or typical peaks due to the lack of any functional groups and since the minute changes due to de-sizing at high temperature may not be observed in the IR spectrum recorded by ATR technique due to poor resolution [42]. The absorption peak for the reference sample at 1582 cm ¹ corresponds to the intrinsic absorption band of graphite materials. Upon acid treating

S. Ayyagari et al.

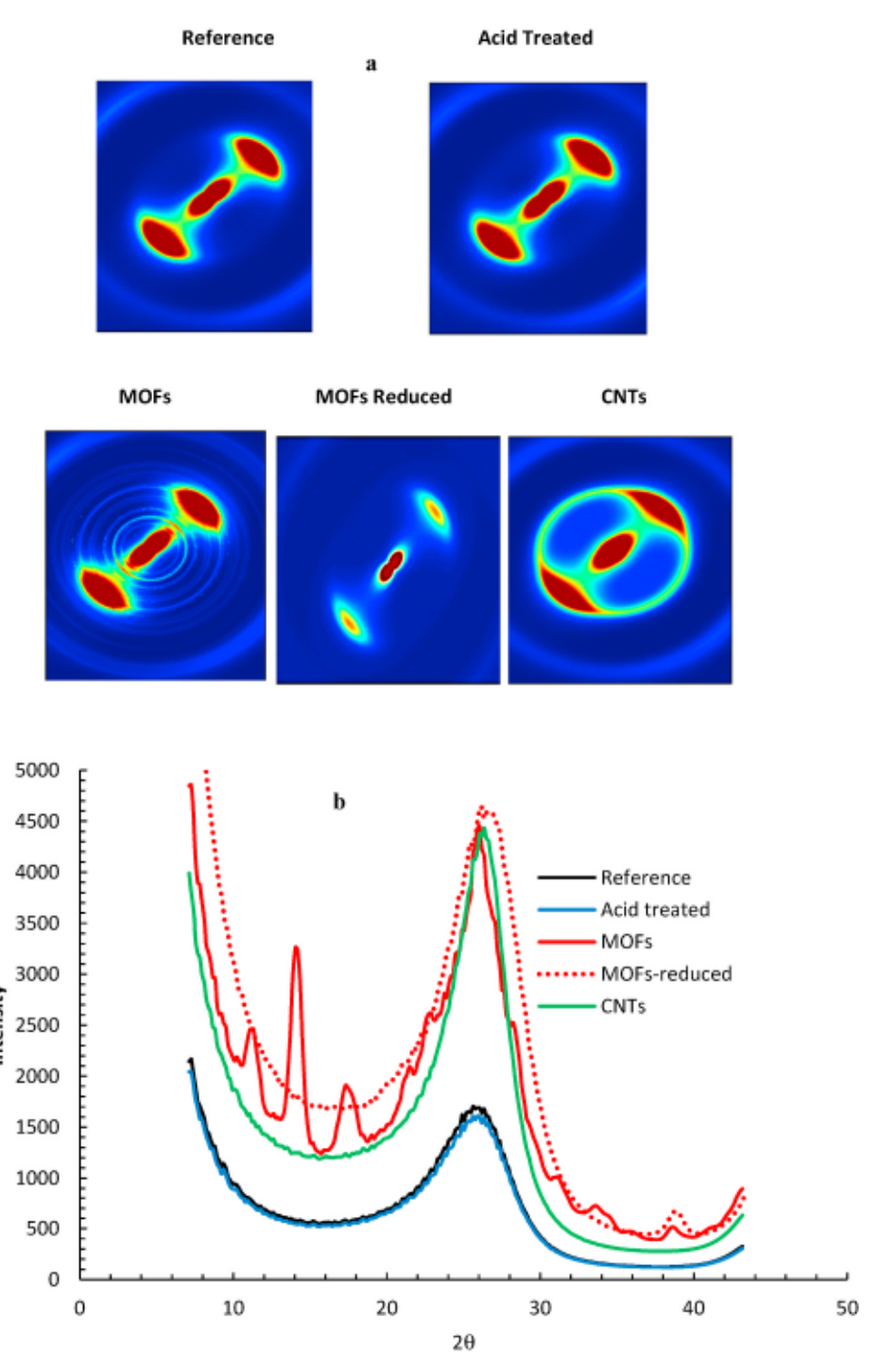


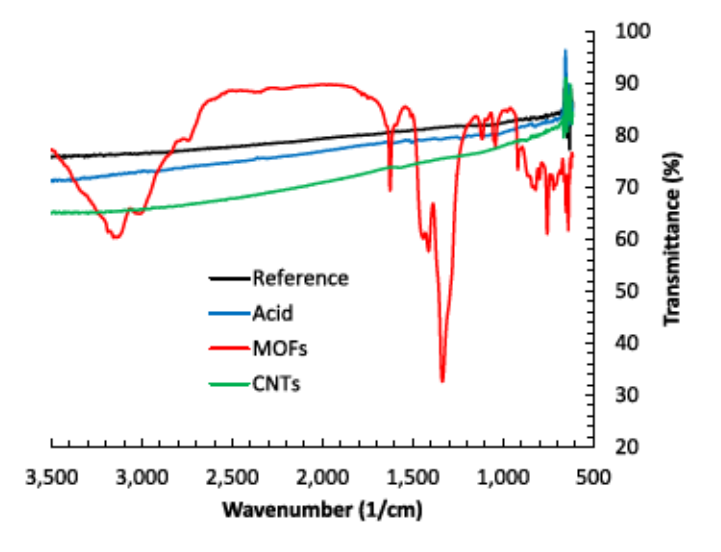
Fig. 4. (a) 2D-WAXD patterns, and (b) WAXD profiles of the T650 fibers after the different surface treatments.

the fiber with diluted nitric acid several new peaks appeared. The groups of G-O-C, C-O-N or C-N appear between 1400 cm⁻¹ and 1000 cm⁻¹ [43]. These peaks are stronger than those of reference carbon fiber, indicating that oxygen functional groups were introduced through oxidation by the nitric acid. The peaks between 3200 and 3500 cm⁻¹ are associated with OH group stretching vibrations [44] indicating water presence due to insufficient drying of the fibers. The FTIR spectra suggest that he deposition of the MOFs on the CF surface was achieved successfully evident by the many peaks that were not seen in the other fiber configurations. The first observation the intense peaks beyond at around 3400 cm⁻¹ is attributed to the O-H group coupling to Ni(ii). The peaks around 1590 and 1390 cm⁻¹ are associated with the stretching of

coordinated carboxylate (-COO') and symmetric stretching mode of coordinated carboxylate, respectively [45]. Finally the peaks between 7500-800 are ascribed to the O-Ni-O vibrations while those around 1050 and 850 cm⁻¹ confirm the C-N and C-H bonds, respectively [46].

Prior to growing CNTs, we investigated the consequences of the thermal reduction of the carbon fibers with MOFs coating under nitrogen environmental at 550 °C for ½ h. Fig. 6 shows a comparison between the morphologies of the MOFs pre and post reduction. The pre-reduction morphology is dominated by interwoven flakes of MOFs, which gives the rise to the walls seen in Fig. 1. The reduced- MOF phase attains particulate shapes with broad particle size distribution. The larger particles morphology suggests they comprise agglomerates of much smaller

8. Ayyagari et al. Composites Part B 224 (2021) 109197



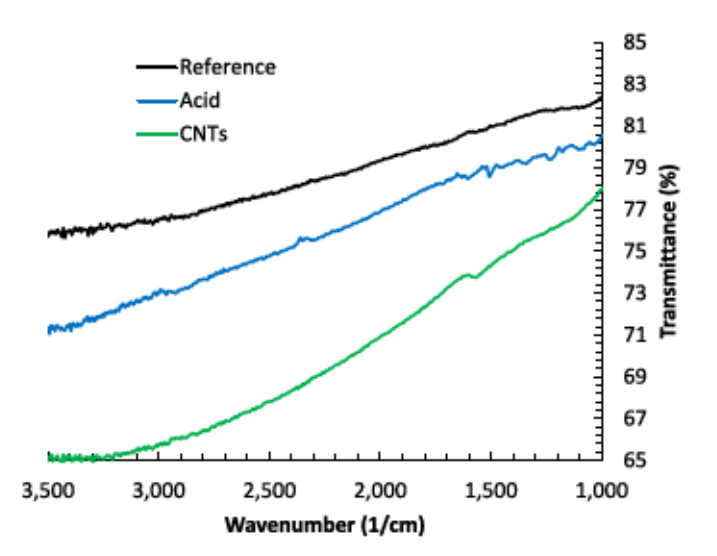


Fig. 5. (a) FTIR Spectra of the different carbon fibers configurations (b) A zoom-in of the spectra of fibers without MOFs.

particles. Utilizing the STEM- BDS mode the composition of these two different phases is given in Table 1. As can be seen, the reduction led to decrease in the carbon content as the organic ingredient of the MOFs decomposed at 550 °C. The reduction procedure achieved its purpose evident by the fact that the oxygen content went down while the nickel percentage increased suggesting removal of oxides which is desirable for

catalytic growth of CNTs.

Utilizing the Image-J ® software, the STEM image was digitized, and a histogram of the particle size distribution was calculated as shown in Fig. 7. There is no dominant size of the reduced particles; they can range from few nm to almost 250 nm. Such wide range of particle size could lead to different CNTs, or even carbon nanofibers, diameters.

The local tow diameter and the meniscus height were recorded by locating the positions of the right and left contact points shown in Fig. 8. The tow was withdrawn from the DI water bath and the weight of the liquid was measured. The contact angle was calculated using the James equation [47] following the procedures outlined in the work by Wang et al. [32]. The water meniscus angles around the different fiber's tows are given in Fig. 8. These results should be considered qualitatively as the fibers tow geometry was changing with time due to capillary induced densification of the tow, which is visible specially in the reference fibers tow. It was observed that the loose fibers in the tow aggregates due to the capillary effect during the immersion in water. However, the level of aggregation was significantly different, the MOFs sample retained almost a constant diameter throughout the immersion process while the other three configurations exhibited a necking in the diameter. The tow with CNTs attained the largest diameter due to the added thickness of the CNTs coating and due to the nanoscale gaps in between the CNTs minimizing the water capillary effect. The evolution of the external water contact angle vs. time for then different fiber tows configuration is shown in Fig. 9. All figures show a quasi-instantaneous meniscus forms evident by the drop of the contact angle from 90° to anywhere between 65° and 45° for the different configurations with MOFs dropping the most. The bend of each curve indicates the time for water to completely fill the tow, where the reference tow attained the shortest time followed by the acid treated, MOFs and the CNTs configuration required much longer time. The phenomenon does not occur instantaneously as water needs to drive the air out. Considering the multiscale capillary effect by the fibers and the CNTs this explains the extended time for water to progress in the CNTs configuration. After the water progressively replaces air in between the fibers in the tow, the contact angle attains its static value. Eventually all different surface treatments aid in reducing the contact angle from 46.31° for the reference fiber tow to 35.07°, 33.43° and 34.52° for the acid treated, MOFs and CNTs configurations, respectively.

The thermal stability of the different fibers' configurations examined via TGA analysis are shown in Fig. 10. The results suggest that the reference sample attained a wt. loss of 10% of the original weight in N₂ environment. Eventually, the lack of a sizing agent or other surface coatings led to such fast and significant degradation. In comparison, literature suggested that sized T650 fiber does not lose more than 2 % wt. under nitrogen environment [48]. The fibers with MOFs coating displayed the fastest degradation rate up to 225 °C, suggesting that most of the weight loss could be attributed to insufficient drying as this sample was soaked separately in water during acid treatment and in

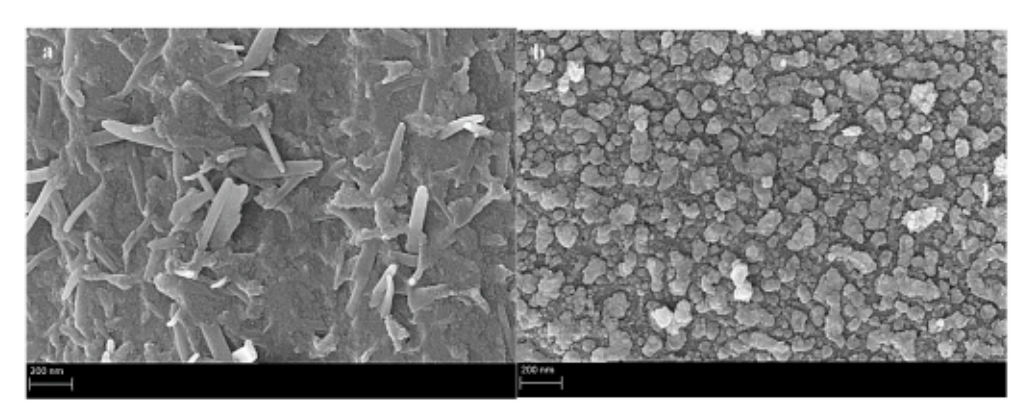


Fig. 6. STEM micrographs of MOFs film deposited on carbon fibers (a) pre and (b) post reduction under nitrogen at 550 °C for 30 min.

Table 1

EDS elemental analysis of MOFs deposited on carbon fiber pre and post reduction under nitrogen environment at 550 C for 30 min. Analysis was taken at 7 different points for each configuration.

	MOPa post reduction (%)				MOF pre redu	MOF pre reduction (%)			
Element	С	N	0	Ni	С	N	0	Ni	
Average	73.08	2.64	4.35	19.93	80.26	3.35	5.05	11.33	
St. Deviation	4.54	0.33	0.38	5.14	5.68	1.43	2.05	2.64	

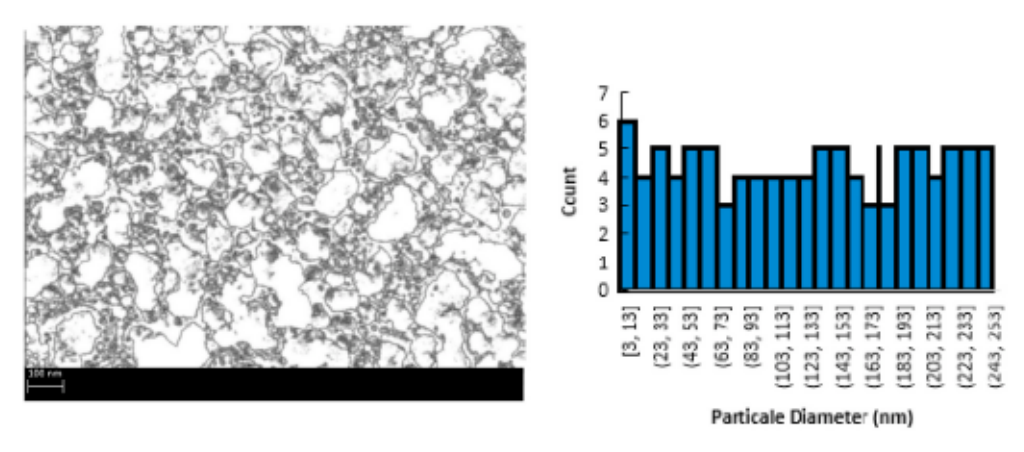


Fig. 7. Image-J® digitized STEM micrograph (b) particle size distribution.

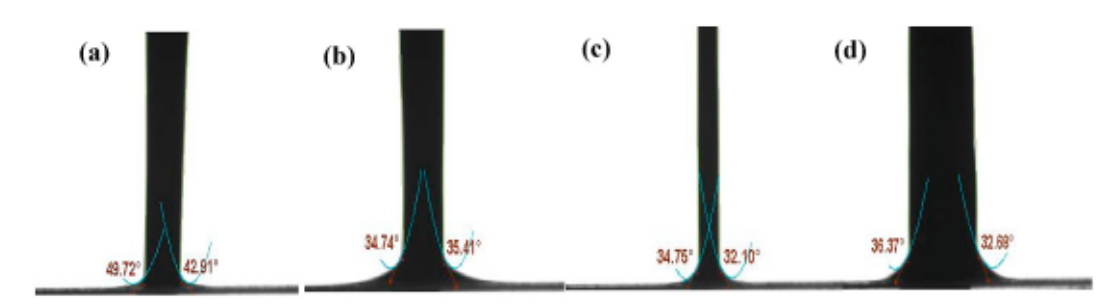


Fig. 8. Comparison of the water meniscus around the different carbon fibers tows configurations; (a) reference, (b) acid treated, (c) MOFs and (d) CNTs. Pictures taken at 100 s after the tow contacted water.

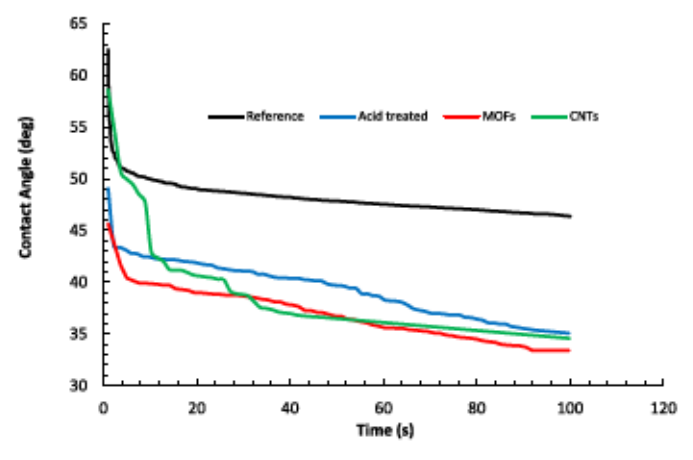


Fig. 9. External water contact angle vs. time for the different carbon fibers tows. The static advancing contact angles were calculated by averaging the angles to the right and left of the fiber axis at the given time.

methanol during the MOFs growth and hence accumulated the most moisture. The rate of degradation beyond that temperature went slower than both the acid treated and the reference sample up to 650 °C, where a higher degradation rate took place suggesting the decomposition of the

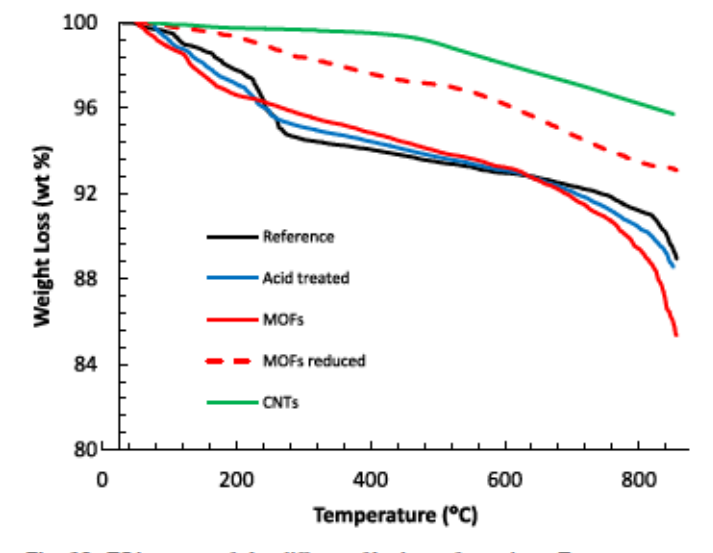
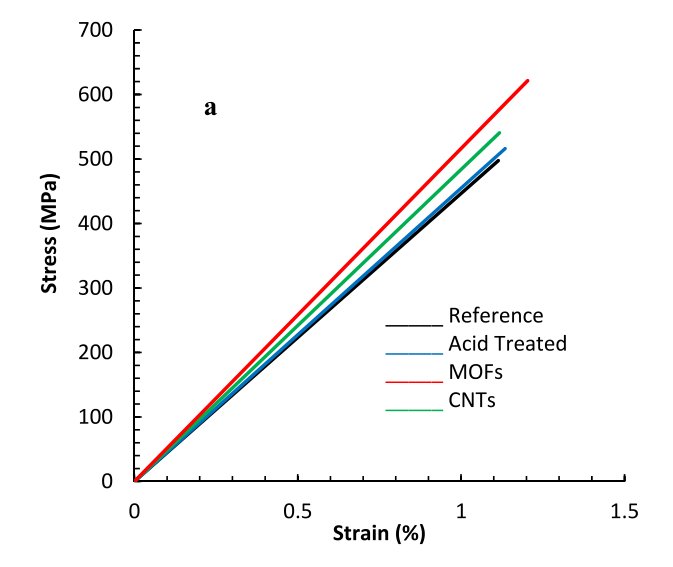


Fig. 10. TGA curves of the different fiber's configurations. Tests were conducted under nitrogen environment.

S. Ayyagari et al. Composites Part B 224 (2021) 109197



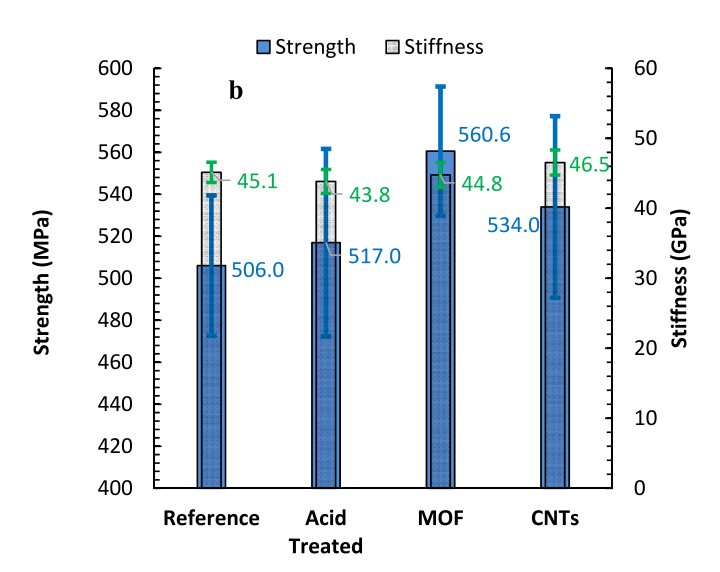


Fig. 11. (a) Representative tensile tests of the composites based on different fiber treatments. (b) The averaged tensile strength and axial stiffness of the composites. Error bars represent the standard deviation.

organic components of the MOFs. This conclusion is reinforced by the minimal degradation pattern of the fiber with MOFs that have undergone a reduction process under nitrogen to produce the nickel particles needed as catalyst to grow the CNTs. This sample has been reduced at 550 C for 30 min, which could have decomposed all the organics from the MOFs structure leaving behind elemental nickel and minimal decomposable compounds leading to less than 6% wt. reduction. This sample is the base sample to grow CNTs, hence, after growing CNTs at 550 C, it maintained better thermal stability at high temperature than any of the other carbon fibers configurations indicating that the grown CNTs have good graphitization structure which was observed by other research groups [49,50].

Fig. 11(a) shows representative tensile tests of the different composite configurations, while Fig. 11(b) summarizes the stiffness and strength for the different composites. From both the figures, it can be observed that all the composite configurations exhibited linear elastic behaviour and the stiffness for all configurations remained almost unaltered. This is mainly because the stiffness is more of a volumetric property that depends on the core of the fiber rather than its surface. The

only configuration to show a slight improvement on the stiffness was that for composites where the fibers are sheathed with CNTs on the surface and that was the only composite where the fibers have been annealed at elevated temperatures which would have sintered the MOF under the CNTs leading to a stiffer phase.

The strength of the composite increased slightly by 2.1% due to acid treatment. The acid treatment in general increases the surface area of the fiber and enhances the surface functionality. The minute increase here is mostly because of the relatively low acid concentration acid (30%), compared to the 60 100% typically utilized to induce significant surface oxidation and noticeable increase in carbon fibers surface area [8,51]. The choice of the low acid concentration was mostly to control the density of MOFs growth in the next steps. It is worth mentioning that some of the previous indicated a reduction of the strength of the carbon fiber itself due to the acid etching [52,53], attributing the damage to the fiber induced by etching as the main cause for strength reduction. This damage was manifested by the decay of the intensity and the broadening in the Raman spectra compared to the reference fiber in Fig. 3. Growing the MOFs on the surface of the fiber increased the strength by 11.0%. The MOFs play significant role in increasing the surface area and providing anchoring between the fiber and the matrix. We hypothesize that the defects induced by the acid etching were filled with MOFs, as the COOH group induced by the acid etching and the ligand in the MOFs play a role in anchoring the Ni-MOF structure to the activated sites on the surface of the carbon fiber. These MOFs assist in better load transition from the matrix to the fiber, and better load distribution on the fiber surface, increasing the load bearing capacity and, thus, enhanced strength. Earlier literature suggested that the fiber themselves become stronger when coated with Zr based or Zn based MOFs after functionalizing the fibers with COOH or NH2 groups through acid treatment [52,53]. Growing CNTs utilizing the Ni-MOFs as catalyst improved the strength of the composite by 5.5%. The increase is less than that for the MOFs because the elevated temperature needed for the CNTs growth induces some damage to the carbon fiber on top of the damage it has encountered due to acid treatment. Growing CNTs uniformly on the carbon fiber often leads to modest increase in the strength. The dense blanket of the CNTs hinders the flow of the epoxy from reaching the underlying carbon fiber, which is crucial for better adhesion and enhanced mechanical properties. We believe that having the MOFs layer beneath the CNTs film still contributes to the improvement on the strength. In a previous investigation [17], we grew CNTs on identical T-650 carbon fiber. However, the Ni catalyst was deposited as uniform smooth film via magnetron sputtering, rather than porous honeycomb film obtained by the MOFs chemistry. In that investigation, we observed only 3.0% improvement on the strength. Hence, the morphology of the MOFs attributed to the better improvement of the composite based on fibers with CNTs, when the MOFs is deposited as the catalyst.

To explore the effects of the different surface treatments on the fiber s/matrix interactions, we examined the micrographs of fractured surfaces of the different tensile samples as shown in Fig. 12. Fig. 12(a b) clearly show that the fracture of the composite based on the reference fibers was dictated by fiber breakage, the absence of strong interface between the fiber and matrix; evident by the clean fiber surface in Fig. 12(b), led to unstoppable crack propagating that propagated across the fiber. Activating the fibers via acid treatment did not change the pattern of fiber failure, but Fig. 12(c d) suggest there was better adhesion evident by the residue of the epoxy on the fiber s surface. Upon growing MOFs, they act as crack deterrents, as shown in Fig. 6(e f). While the cracks initiated in matrix zone, upon further loading, they get deflected along the axis of the fibers on a wavy trajectory that can be clearly seen in Fig. 12(e). The MOFs stay intact to the fiber surface, manifested by the shiny surface of the fiber as seen in Fig. 12(f). Fig. 12 (g) suggests that the existence of CNTs at the interface hinders crack propagation along the fiber axis and the matrix in between. Adjacent fibers did not undergo longitudinal crack propagation as well. Very S. Ayyagari et al. Composites Part B 224 (2021) 109197

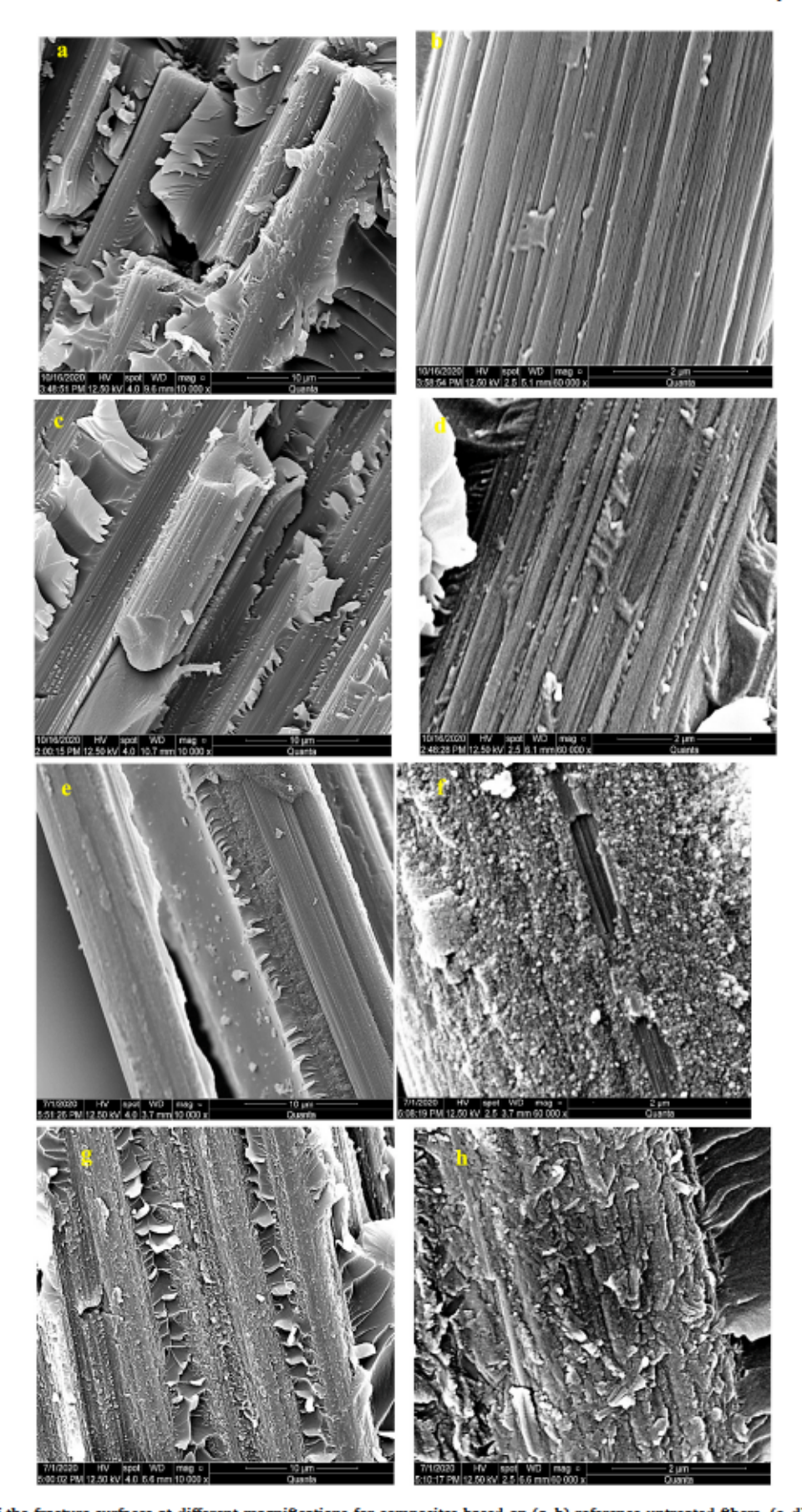


Fig. 12. Micrographs of the fracture surfaces at different magnifications for composites based on (a-b) reference untreated fibers, (c-d) acid treated fibers, (e-f) fibers with MOFs, and (g-h) fibers with surface grown CNTs utilizing the MOFs as catalyst.

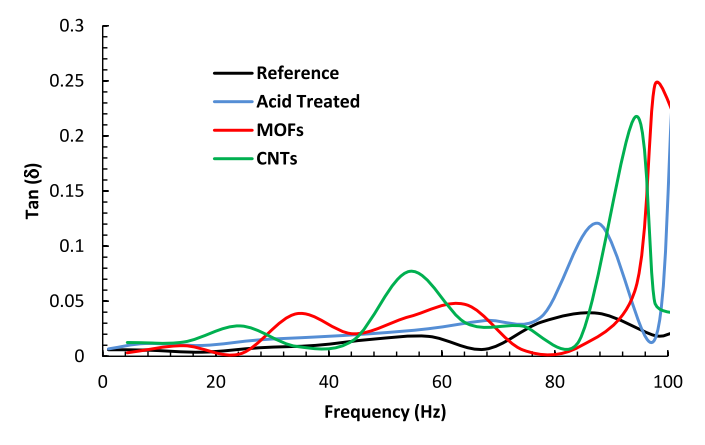


Fig. 13. The DMA measurements of the damping parameter; tan () for the different composites configurations via frequency sweep at room temperature.

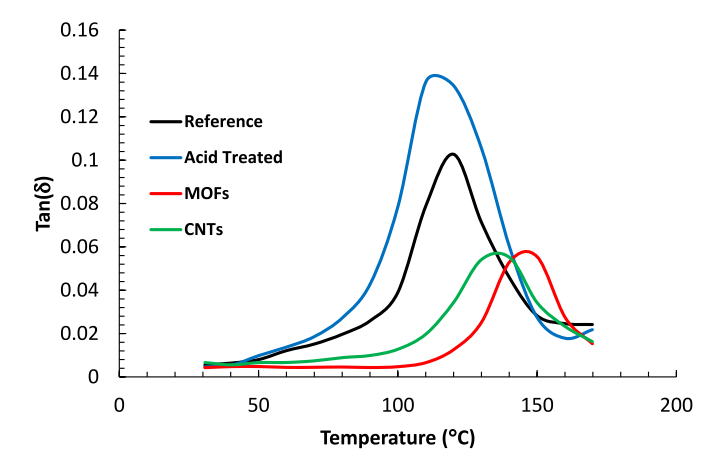
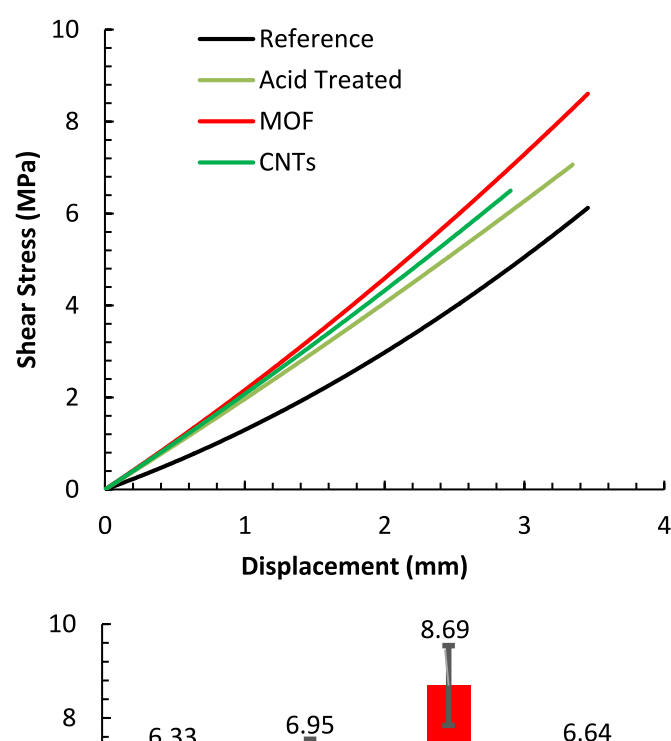


Fig. 14. DMA temperature sweep for composites based on reference, acid treated, MOF modified and CNTs growth carbon fibers. Measurements conducted at a frequency of 1.0 Hz.

rough fracture surfaces were observed in Fig. 12(h) indicating good adhesion between the fibers and the matrix. For both composites based on MOFs and CNTs, the composite exhibited little or no cracks in between the fiber, suggesting that the patterned deposition of the MOFs, and the consequent CNTs growth, promoted mechanical interlocking mechanism between the nano reinforcement species and the epoxy matrix constituting strong impediments which inhibited crack propagation and, thus, yielded enhanced strength.

The DMA frequency sweep results are shown in Fig. 13 in terms of the damping parameter tan (). To conceive these results, it is crucial to consider the different mechanisms that affect the damping capacity of FRPs, such as interfacial bonding, stick-slip friction, and nano fillers additives [54]. Clearly, the FRPs based on the reference carbon fibers attained the lowest damping parameter. The composite based on the fibers functionalized with nitric acid showed an improvement in damping by as much as 200% at 87 Hz, since the diluted acid treatment enhanced the surface area of the carbon fiber, evident by fibril like striation on the surface Fig. 1(b), allowing for larger contact with the epoxy and hence larger energy dissipation. Furthermore, the weakened graphitic outer layers of the fiber could have also promoted the stick-slip mechanism the fiber matrix interface. The addition of the MOFs to the fiber surface increases the surface area even further, and the weak epoxy-metal interfacial bonding allows for more energy dissipation and thus the damping parameter increased as high as 500% over the composite based on the reference fiber. The growth of CNTs on the carbon fibers increases the surface area tremendously due to the high aspect



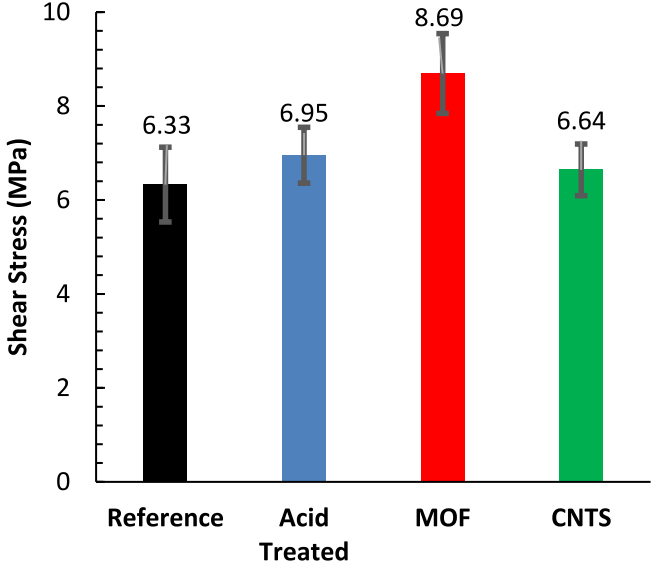


Fig. 15. (a) Representative shear lap joint stress vs. displacement for the different composites configurations, and (b) the effect of surface treatment method on bond adhesive shear strength.

ratio of the CNTs. This new added interface area allows for significant friction between the CNTs and the epoxy leading to significant energy dissipation. Furthermore, from the tensile tests, it was evident that the placement of the CNTs at the interface allows for a better stiffness which is consistent with the hypothesis of sliding taking place at the CNTs/matrix interface [54]. The combination of all these attributes allowed the composite with CNTs to attain an improvement of the damping coefficient by up to 425%.

The DMA analysis can also elucidate how the different fiber s surface treatments can affect the glass transition temperature, $T_{\rm g}$, of the FRP. A widely accepted measure of the glass transition temperature is the peak of tan() curves [55,56]. From Fig. 14 the $T_{\rm g}$ for the composite based on the reference sample is about 120 $\,$ C and is increasing to 140 $\,$ C and 150 $\,$ C with the surface treatments with MOFs and CNTs, respectively. No significant change was observed for the composites based on acid treated fibers. The results suggest that the interface embodied by a new phase between the fiber and matrix plays crucial role in the shift of the glass transition temperature. Both the MOFs and the CNTs constitute obstacles that could hinder the epoxy. During glass transition, the epoxy

8. Ayyagari et al. Composites Part B 224 (2021) 109197

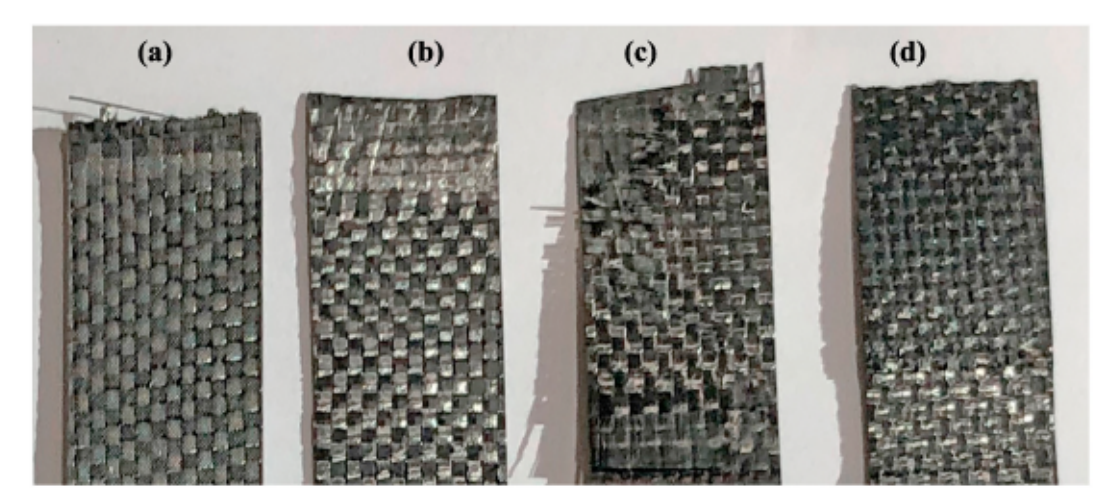


Fig. 16. Representative images of the different joint failure modes observed for composites based on (a) reference fibers (b) acid treated fibers, (c) fibers with MOF, and (d) fibers with surface grown CNTs.

molecular chains absorb thermal energy and start moving. However, having the MOFs and CNTs on the surface of the fiber slow down this movement, without diminishing it. Thus, more energy (and thus higher temperature) is needed to overcome these nanoscale hurdles. Although the glass transition is an intrinsic property of the polymer matrix, it is clearly affected by the fiber presence and the fiber's surface treatment. A previous investigation [56] suggested that the mere presence of the fibers do not affect the Tg along the fiber direction, but slightly reduces the To along the fiber transverse direction. This indirectly correlates the Te to the strength and stiffness, as these properties reach their maximum along the fiber direction and attain their minimum values in the transverse direction. In support of this hypothesis, another investigation found that increasing the fiber volume fraction in an epoxy, hence the strength and stiffness, could increase the glass transition by as much as 25 °C [57]. Thus, the results of the current study suggest that the measurement of Tg could offer a venue to, qualitatively, probe the effects of fiber surface treatment on the mechanical performance of epoxy-based composites.

Fig. 15(a) displays representative strength-displacement curves for the four different composites, with single-lap bonded joints, while Fig. 15(b) summarizes the average joint shear strengths. The composite based on the reference fiber exhibited the lowest joint shear strength. To classify the failure mode of the joints, we examined the joint area after failure consulting the ASTM standard D5573. Fig. 16(a) shows that the composite based on the reference fibers exhibited a stock-break failure as the sample broke outside the joint area. The acid treatment of the fiber improved the adhesion shear strength by 10%. This increase is attributed to the enhanced surface roughness of the fiber, due to the acid induced roughening of the carbon fibers. The sample based on the acid treated fibers displayed a cohesive failure evident by Fig. 16(b) as the adhesive layer separated such that its residue appeared at both surfaces of the joint. It was believed that for carbon fibers oxidized via nitric acid treatments, it is the surface functionality rather than the increase in surface area that is responsible for improvements of the shear strength [58]. In particular, the number of the bonds per unit length formed between the resin molecules and the surface groups induced by acid treatment on the surface of the carbon fibers, rather than the concentration of the bonds or the surface area is responsible for such

The composite based on fibers with MOF displayed a remarkable improvement in the adhesive joint shear strength; 40%. The nanosheet structures of the MOFs are responsible for this improvement through furnishing an extended contact area and a mechanical interlocking of the epoxy between the MOFs pores. This sample displayed a fiber-tear failure, as the failure resulted in the appearance of reinforcing fibers

on both ruptured surfaces as shown in Fig. 16(c). The tearing of the fibers within the joint is indicative of significant shear bearing capability. Finally, for the composite based on carbon fiber with surface grown CNTs, the shear lap strength improvement was minute and was limited to 4.4%. Fig. 16(d) reveals that the epoxy did not wet the CNTs well, despite the elevated pressure in the autoclave, due to the dense growth of the CNTs. This resulted in a thin-layer cohesive failure, where some adhesive dusting can be seen on one of the joint surfaces and a thicker layer on the opposite surface. Our previous investigations were able to improve the shear strength of FRPs only when CNTs were grown in patterned patches to allow for the epoxy to flow in between these patches [17]. Previous work [59] suggested that for a shear lap test, the CNTs contribute better improvements to the FRPs when a surfactant is utilized to activate them prior to their dispersion in the epoxy matrix to form a better adhesive paste.

4. Conclusions

This investigation provides a practical route for enhancing the interfacial, mechanical, and dynamic properties of FRPs by utilizing scalable, yet tailorable synthesis of MOFs on carbon fiber reinforcements, prior to composites fabrication. The MOFs furnish the fibers with significant increase in the interfacial area to ensure better adhesion to the epoxy matrix. This is accompanied with several bonding and chemical groups revealed by the FTIR analysis. The synthesis technique yields crystalline Ni based MOFs that are also suitable as catalysts for growing CNTs to add more functionality to the composite. The growth can be tailored to control both the amount and the porosity of the MOFs; significant MOF growth leads to dense CNTs growth as it substantiates a continuous source of Ni catalyst needed for the CNTs growth.

Tensile results suggests that MOFs outperforms other surface treatments, such as acid functionalizing of the carbon fibers, in improving the strength by furnishing new surface area and by acting as mechanical anchors in the epoxy matrix. The enhancement in strength arises from both physical and chemical sources. The FTIR analysis revealed that the MOFs have far more chemical bonding to the fibers than any of the other configurations including —COOH group and several Ni—O bonds. Also, the MOFs tend to enhance the fiber hydrophilicity evident by the reduced angle of contact. Finally, the interlocking of the epoxy between the MOFs pores increases the interface with the epoxy leading to better adhesion and strength.

Adding MOFs to the carbon fibers also assisted in a significant shift of the Tg of the composite by 20 °C compared to composites based on the pristine fibers. The damping performance of the fiber/MOFs hybrid S. Ayyagari et al. Composites Part B 224 (2021) 109197

composite outperformed all other configurations, including those incorporating CNTs, yielding a damping parameter improvement of 500%

The most noticeable improvement induced by the MOFs is that for the shear lap joint strength, as the MOFs based hybrid composite yielded 40% improvements in the shear strength of the joint. These preliminary results lay the foundation for next generation of hybrid composites that can contribute to several functionalities in FRPs, while offering remedies to the root cause of failure in composites: poor interfacial adhesion between the fibers and the matrix.

Declaration of competing interest

The authors declare that they have no known competing financial interests or personal relationships that could have appeared to influence the work reported in this paper

Acknowledgments

This research has been supported by the Air Force Research Laboratory (AFRL), Summer Faculty Fellowship Program (SFFP-2020) to Dr. Al-Haik. Dr. Al-Haik also acknowledges the support from the National Science Foundation Grants CMMI - 2001038 and CMMI 2018375.

References

- Ivanov Y, Cheshkov V, Natova M. Polymer composite materials interface phenomena and processes. Dordrecht, The Netherlands: Kluwer Academic Publishers; 2001.
- [2] Kim JK, Mai YW. Engineered interfaces in fiber reinforced composites. Oxford, UK: Elsevier Science Ltd.; 1998.
- [3] Di Boon Y, Joshi SC. A review of methods for improving interlaminar interfaces and fracture toughness of laminated composites. Mater Today Commun 2020;22.
- [4] Jesson DA, Watts JF. The interface and interphase in polymer matrix composites: effect on mechanical properties and methods for identification. Polym Rev 2012;52 (3.4):321–54
- [5] Jones FR. A review of interphase formation and design in fibre-reinforced composites. J Adhes Sci Technol 2010;24(1):171 202.
- [6] Shin PS, Kim JH, Park H, Baek YM, Lee SI, DeVries KL, et al. A review: mechanical and interfacial properties of composites after diverse types of aging using micromechanical evaluation. Fibers Polym 2020;21(2):225–37.
- [7] Chiang YC, Lee CC, Lee HC. Characterization of microstructure and surface properties of heat-treated PAN-and rayon-based activated carbon fibers. J Porous Mater 2007;14(2):227–37.
- [8] Wu GM, Hung CH, You JH, Liu SJ. Surface modification of reinforcement fibers for composites by acid treatments. J Polym Res 2004;11(1):31 6.
- [9] Andideh M, Esfandeh M. Effect of surface modification of electrochemically oxidized carbon fibers by grafting hydroxyl and amine functionalized hyperbranched polyurethanes on interlaminar shear strength of epoxy composites. Carbon 2017;123:233 42.
- [10] Fu YP, Li HX, Cao WY. Enhancing the interfacial properties of high-modulus carbon fiber reinforced polymer matrix composites via electrochemical surface oxidation and grafting. Compos Appl Sci Manuf 2020:130.
- [11] Alamer FA, Badawi NM, Alsalmi O. Preparation and characterization of conductive cotton fabric impregnated with single-walled carbon nanotubes. J Electron Mater 2020;49:6582 9.
- [12] Ayyagari S, Al-Haik M. Enhancing the viscoelastic performance of carbon fiber composites by incorporating CNTs and ZnO nanofillers. Appl Sci 2019;9(11).
- [13] Boroujeni AY, Al-Haik M, Emami A, Kalhor R. Hybrid ZnO nanorod grafted carbon fiber reinforced polymer composites; randomly versus radially aligned long ZnO nanorods growth. J Nanosci Nanotechnol 2018;18(6):4182 8.
- [14] Yao ZQ, Wang CG, Qin JJ, Su SS, Wang YX, Wang QF, et al. Interfacial improvement of carbon fiber/epoxy composites using one-step method for grafting carbon nanotubes on the fibers at ultra-low temperatures. Carbon 2020;164: 133 42.
- [15] Sager RJ, Klein PJ, Lagoudas DC, Zhang Q, Liu J, Dai L, et al. Effect of carbon nanotubes on the interfacial shear strength of T650 carbon fiber in an epoxy matrix. Compos Sci Technol 2009;69(7–8):898–904.
- [16] Abidin AZ, Kozera R, Hohn M, Endler I, Knaut M, Boczkowska A, et al. Preparation and characterization of CVD-TiN-coated carbon fibers for applications in metal matrix composites. Thin Solid Films 2015;589:479 86.
- [17] Ayyagari S, Al-Haik M, Ren YX, Nepal D. Effect of nano-reinforcement topologies on the viscoelastic performance of carbon nanotube/carbon fiber hybrid composites. Nanomaterials 2020;10(6).
- [18] Boroujeni AY, Al-Haik M. Carbon nanotube carbon fiber reinforced polymer composites with extended fatigue life. Compos B Eng 2019;164:537 45.

[19] Boroujeni AY, Al-Haik MS. Interlaminar fracture toughness of hybrid carbon fibercarbon nanotubes-reinforced polymer composites. Polym Compos 2019;40: E1470 8.

- [20] MacGillivray LR, Lukehart CM. Metal-organic framework materials. West Sussex, UK: John Wiley & Sons Ltd; 2014.
- [21] Tran TQN, Das G, Yoon HH. Nickel-metal organic framework/MWCNT composite electrode for non-enzymatic urea detection. Sensor Actuator B Chem 2017;243: 78, 83
- [22] Yan LT, Jiang HM, Xing YL, Wang Y, Liu DD, Gu X, et al. Nickel metal-organic framework implanted on graphene and incubated to be ultrasmall nickel phosphide nanocrystals acts as a highly efficient water splitting electrocatalyst. J Mater Chem 2018;6(4):1682–91.
- [23] Bhoria N, Basina G, Pokhrel J, Reddy KSK, Anastasiou S, Balasubramanian VV, et al. Functionalization effects on HKUST-1 and HKUST-1/graphene oxide hybrid adsorbents for hydrogen sulfide removal. J Hazard Mater 2020;394:11.
- [24] Kim HR, Yoon TU, Kim SI, An J, Bae YS, Lee CY. Beyond pristine MOFs: carbon dioxide capture by metal-organic frameworks (MOFs)-derived porous carbon materials. RSC Adv 2017;7:1266 70.
- [25] Tedds S, Walton A, Broom DP, Book D. Characterisation of porous hydrogen storage materials: carbons, zeolites, MOFs and PIMs. Farady Discuss. 2011;151: 75–94.
- [26] Liu Y, Xu J, Liu SC. Porous carbon nanosheets derived from Al-based MOFs for supercapacitors. Microporous Mesoporous Mater 2016;236:94 9.
- [27] Meng XH, Wan CB, Yu SY, Jiang XP, Ju X. Nickel/porous carbon composite derived from bimetallic MOFs for electrical double-layer supercapacitor application. Int J Electrochem Sci 2018;13:8179 88.
- [28] Liu YZ, Li GR, Guo Y, Ying YL, Peng XS. Flexible and binder-free hierarchical porous carbon film for supercapacitor electrodes derived from MOFs/CNT. ACS Appl Mater Interfaces 2017;9:14043 50.
- [29] Zheng GX, Chen MH, Zhang HR, Zhang JW, Liang XQ, Qi ML, et al. Zn-MOFs derived porous carbon nanofiber for high performance lithium-ion batteries. Surf Coating Technol 2019;359:384 9.
- [30] Chen K, Sun Z, Fang R, Shi Y, Cheng HM, Li F. Metal-organic frameworks (MOFs)-Derived nitrogen-doped porous carbon anchored on graphene with multifunctional effects for lithium-sulfur batteries. Adv Funct Mater 2018;28:1707592.
- [31] Heiney P. Datasqueeze: A software tool for powder and small-angle X-ray diffraction analysis. Comm Powder Diffr Newsl 2005;32:9 11.
- [32] Wang J, Fuentes CA, Zhang D, Wang X, Vuure AWV, Seveno D. Wettability of carbon fibres at micro- and mesoscales. Carbon 2017;120:438 46.
- [33] Rahmani H, Ashori A, Varnaseri N. Surface modification of carbon fiber for improving the interfacial adhesion between carbon fiber and polymer matrix. Polym Adv Technol 2016;27:805 11.
- [34] Zhong YX, Cao XY, Liu Y, Cui L, Barrow C, Yang WR, et al. Homogeneous nickel metal-organic framework microspheres on reduced graphene oxide as novel electrode material for supercapacitors with outstanding performance. J Colloid Interface Sci 2020:561:265-74.
- [35] Aslam S, Subhan F, Yan ZF, Etim UJ, Zeng JB. Dispersion of nickel nanoparticles in the cages of metal-organic framework: an efficient sorbent for adsorptive removal of thiophene. Chem Eng J 2017;315:469 80.
- [36] Bao CC, Niu QQ, Chen ZA, Cao XW, Wang H, Lu WB. Ultrathin nickel-metalorganic framework nanobelt based electrochemical sensor for the determination of urea in human body fluids. RSC Adv 2019;9(50):29474 81.
- [37] Fitzer E. PAN-based carbon fibers-present state and trend of the technology from the viewpoint of possibilities and limits to influence and to control the fiber properties by the process parameters. Carbon 1989;27(5):621 45.
- [38] Woodhead AL, Souza MLd, Church JS. An investigation into the surface heterogeneity of nitric acid oxidized carbon fiber. Appl Surf Sci 2017;401:79–88.
- [39] Krylov A, Vtyurin A, Petkov P, Senkovsk I, Maliuta M, Bon V, et al. Raman spectroscopy studies of the terahertz vibrational modes of a DUT-8 (Ni) metal organic framework. Phys Chem Chem Phys 2017;19:32099 104.
- [40] Gupta A, Harrison I, Lahijani J. Small-Angle X-Ray scattering in carbon fibers. J Appl Cryst 1994;27:627–36.
- [41] Tang MY, Rice GG, Fellers JF, Lin JS. X-ray scattering studies of graphite fibers. J Appl Phys 1986;60:803 10.
- [42] Boccara AC, Fournier D, Kumar A, Pandey GC. Nondestructive evaluation of carbon fiber by mirage FTIR spectroscopy. J Appl Polym Sci 1997;63:1785 91.
- [43] Wang L, Liu N, Guo Z, Wu D, Chen W, Zhang Z, et al. Nitric acid-treated carbon fibers with enhanced hydrophilicity for Candida tropicalis immobilization in xylitol fermentation. Materials 2016;9:206–16.
- [44] Pamula E, Rouxhet PG. Bulk and surface chemical functionalities of type III PAN-based carbon fibres. Carbon 2003;41:1905 15.
- [45] Ahsan MA, Jabbari V, Imam MA, Castro E, Kim H, Curry ML, et al. Nanoscale nickel metal organic framework decorated over graphene oxide and carbon nanotubes for water remediation. Sci Total Environ 2020;698:134214 25.
- [46] Mousavinejad A, Rahimpour A, Kebria MR, Salestan SK, Sadrzadeh M, Kiadeh NT. A nickel-based metal organic framework to improve the CO2/CH4 separation capability of thin film pebax membranes. Ind Eng Chem Res 2020;59:12834 44.
- [47] James DF. The meniscus on the outside of a small circular cylinder. J Fluid Mech 1974;63:657 64.
- [48] Zhang Q, Liu J, Sager R, Dai L, Baur J. Hierarchical composites of carbon nanotubes on carbon fiber: influence of growth condition on fiber tensile properties. Compos Sci Technol 2009;69:594 601.
- [49] Mathur RB, Chatterjee S, Singh BP. Growth of carbon nanotubes on carbon fibre substrates to produce hybrid/phenolic composites with improved mechanical properties. Compos Sci Technol 2008;68:1608 15.

- [50] Qin J, Wang C, Wang Y, Su S, Yao Z, Ma Z, et al. Preparation carbon nanotube-decorated carbon fibers under low pressure for epoxy-based unidirectional hierarchical composites with enhanced interlaminar shear strength. Polym Test 2021;93:106892-01.
- [51] Shim JW, Park SJ, Ryu SK. Effect of modification with HNO and NaOH on metal adsorption by pitch-based activated carbon fibers. Carbon 2001;39:635–1642.
- [52] Li Y, Jiang B, Huang Y. Constructing nanosheet-like MOF on the carbon fiber surfaces for improving the interfacial properties of carbo fiber/epoxy composites. Appl Surf Sci 2020;514:145870.
- [53] Yang X, Jiang X, Huang Y, Guo Z, Shao L. Building nanoporous metal organic frameworks armor on fibers for high-performance composite materials. Appl Mater Interfaces 2017;9:5590 9.
- [54] Tang X, Yan X. A review on the damping properties of fiber reinforced polymer composites. J Ind Textil 2018;49:693 721.

- [55] Goertzen WK, Kessler MR. Creep behavior of carbon fiber/epoxy matrix composites. Mater Sci Eng 2006;421:217 25.
- [56] Bussu G, Lazzeri A. On the use of dynamic mechanical thermal analysis (DMTA) for measuring glass transition temperature of polymer matrix fibre reinforced composites. J Mater Sci 2006;41:6072 6.
- [57] Dong S, Gauvin R. Application of dynamic mechanical analysis for the study of the interfacial region in carbon fiber/epoxy composite materials. Polym Compos 1993; 14:414 20.
- [58] Brooks CS, Golden GS, Scola DA. Characterization of surface reactivity of graphite fiber by solute adsorption. Carbon 1974;12:609 17.
- [59] Hsiao KT, Alms J, Advani SG. Use of epoxy/multiwalled carbon nanotubes as adhesives to join graphite fibre reinforced polymer composites. Nanotechnology 2003;14:791 3.